Journal of Alloys and Compounds 509 (2011) 854–858

Contents lists available at ScienceDirect

Journal of Alloys and Compounds

journal homepage: www.elsevier.com/locate/jallcom

Nanopowder synthesis of aluminum doped cadmium oxide via sol–gel calcination processing

C. Aydın[a], H.M. El-Nasser[b], F. Yakuphanoglu[a,c,*], I.S. Yahia[a,d], M. Aksoy[a]

[a] Metallurgical and Materials Science Engineering Department, Firat University, Elazig, Turkey
[b] Department of Physics, Al al-Bayt University, Mafraq-Jordan, Jordan
[c] Department of Physics, College of Science, King Saud University, Riyadh, Saudi Arabia
[d] Physics Department, Faculty of Education, Ain Shams University, Roxy, Cairo, Egypt

ARTICLE INFO

Article history:
Received 1 September 2010
Received in revised form 9 September 2010
Accepted 19 September 2010
Available online 25 September 2010

Keywords:
Pure and Al-doped CdO nanostructure
Sol–gel
Diffused reflectance
Optical band gap
Dc electrical conductivity

ABSTRACT

The structural, optical and electrical properties of undoped and Al-doped CdO powder nanostructures prepared by sol–gel calcinations method have been investigated. X-ray diffraction (XRD) results revealed that pure and Al-doped CdO have the polycrystalline with face centered cubic (FCC) structure. The crystallite size for undoped and 5, 10, 15, 20% of Al-doped CdO samples were found to be 17.2, 15.9, 16.1, 16.3 and 16.8 nm, respectively. The optical band gap of the samples were determined from the diffused reflectance spectra and E_g values for undoped and 5, 10, 15, 20% of Al-doped CdO samples were found to be 1.89, 2.07, 2.03, 2.07 and 2.12 eV, respectively. The electrical conductivities of pure and Al-doped CdO were measured in the temperature range (290–420 K) and their temperature dependence was analyzed according to Arrhenius relation. The electrical conductivity results indicate that the electrical conductivity mechanism is controlled by thermally activated processes. The results showed that sol–gel calcinations technique can be effectively used to produce undoped and doped nanopowders.

1. Introduction

Thin films of transparent conductive oxides (TCO) such as zinc oxide, indium–tin oxide, tin oxide and cadmium oxide have been extensively studied because of their use in semiconductor optoelectronic device applications [1]. In recent years, the metal oxide semiconductor materials have attracted much attention owing to their potential applications in electronic and photovoltaic devices. CdO is *n*-type semiconductor with a rock-salt crystal structure (FCC) and possesses a direct band gap of 2.2 eV. Its high optical transmittance in the visible region of the solar spectrum along with a moderate refractive index make it useful for various applications such as solar cells, transparent electrodes, phototransistors, photodiodes, gas sensors, etc. [2,3]. CdO has received a considerable attention as the transparent electrode of CdTe-based thin film solar cells because its electro-optical properties compare with those of the traditional TCOs [4]. But, cadmium oxide is not a popular TCO material due to its low optical band gap. While, CdO is a particularly interesting material because it is one of the semiconducting oxides with high carrier mobility, and has great potential for using in optoelectronic devices.

CdO has a great technological interest due to their high-quality electrical and optical properties. Doped CdO with different dopants (F, In, Ga, Al, Fe, Cd, Zn, etc.), as multicomponent oxides constituted of CdO, have been used in several applications: photovoltaic devices, gas sensors, phototransistors and diodes, etc. [5,6]. Different methods have been adopted to deposit doped and pure CdO films such as metalorganic chemical vapor deposition (MOCVD), sputtering [7], electron beam evaporation [8], sol–gel [9,10], pulsed laser deposition [11], dc magnetron sputtering [12], radio-frequency sputtering [13], spray pyrolysis [14], and chemical bath deposition [15].

Among this methods of preparation pure and doped CdO, the sol–gel route method is one of the most promising available methods for synthesizing nanoparticles of controlled size and morphology. The sol–gel technique is one of the most promising tools in material science. The versatility of this method allows us to design desired materials at the lower temperatures, alternatively to conventional methods for manufacturing materials. The synthetic route provided by this system is the most feasible one for designing materials possessing unique properties. Generally, it is a process concerning transition of a system from liquid 'sol' (the colloidal suspension of particles) into solid 'gel'. On the other hand sol–gel technique is simpler and cost-effective. Accordingly, this method is adopted and applied to sensitize both of pure and Al-doped CdO nanostructures in the present study.

* Corresponding author.
E-mail addresses: fyhanoglu@firat.edu.tr, fyakuphanoglu@ksu.edu.sa (F. Yakuphanoglu).

0925-8388/$ – see front matter © 2010 Elsevier B.V. All rights reserved.
doi:10.1016/j.jallcom.2010.09.111

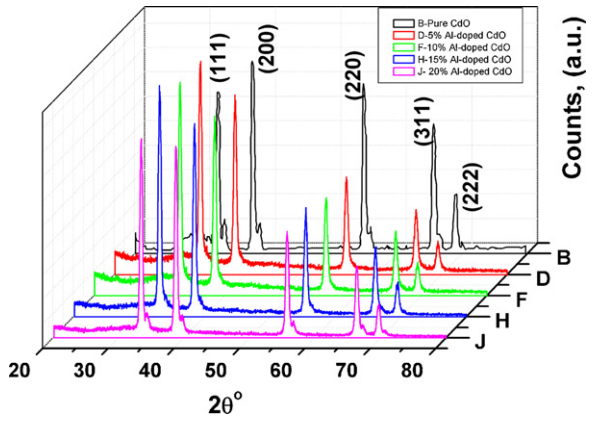

Fig. 1. XRD patterns for (B) pure CdO, (D) 5%, (F) 10%, (H) 15% and (J) 20% Al-doped CdO powder nanostructures.

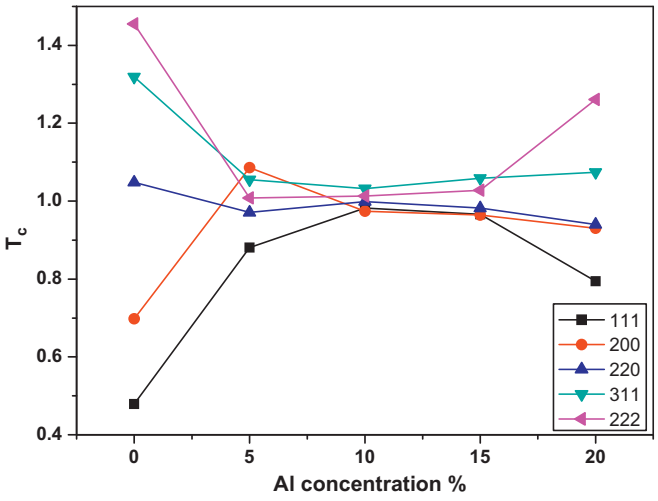

Fig. 2. The plot of T_c as a function of Al concentrations for different planes.

In present work, we have synthesized pure and Al-doped CdO by sol–gel calcinations route. X-ray diffraction patterns were used to identify the phases of pure and Al-doped CdO. Diffused reflectance as a new method was used to characterize the optical band gap of the powder samples. Dc electrical conductivity was studied to analyze the electrical conduction mechanism.

2. Experimental

2.1. Preparation of the samples

Solutions of undoped and Al–doped CdO were prepared by sol–gel route method as follows: Undoped CdO precursor solution was prepared by the following procedure: (i) the cadmium acetate was dissolved in 2-methoxyethanol (MTE) (0.5 M) at a constant magnetic stirring for 10 min and then, monoethanolamine (0.5 M) (C_2H_7NO, MEA) as stabilizer was added to the solution during the stirring; (ii) The solution was stirred constantly for two hours. CdO precursor containing Al-dopants were prepared as follows: (0.5 M) cadmium acetate and (0.5 M) with different percents (5, 10, 15 and 20%) aluminum nitrate ($Al(NO_3)_2{\cdot}9H_2O$), were dissolved in MTE for 10 min. Afterwards, MEA was added drop by drop with continuous stirring and the final solution was stirred for 2 h at 60 °C. The obtained gels were calcinated in a tube furnace for 2 h at 700 °C, respectively. The powders samples were prepared in form of disc to characterizations.

2.2. Characterization

X-ray diffraction patterns of the samples were obtained with a D8 BRUKER X-ray diffractometer using CuKα radiations (λ = 1.54059 Å). The structural properties of the powder samples were investigated by Park System XE-100E atomic force microscopy (AFM). The diffuse reflectance spectra of the investigated samples were performed using a Shimadzu UV-VIS-NIR 3600 spectrophotometer using an integrating sphere attachment.

3. Results and discussion

3.1. Structural properties of pure and Al-doped CdO nanostructures

The XRD patterns of pure and Al-doped CdO nanostructure powder samples are shown in Fig. 1. The different peaks in the XRD pattern of the samples were appeared at 2θ values, 32.995°, 38.292°, 55.260°, 65.921° and 69.293° corresponding to (1 1 1), (2 0 0), (2 2 0), (3 1 1) and (2 2 2) reflections, respectively. XRD patterns revealed that pure and Al-doped CdO have faced centered cubic (FCC) structure. The relatively stronger intensity peaks at $2\theta^\circ$ equal 32.995 and 38.292, in which their intensities were changed by Al dopant. It is clear that the preferred orientation changes from (1 1 1) to (2 0 0) plane with changing the Al doping. The same behaviour was observed in the pure and Al-doped CdO prepared by pulsed laser deposition and by sol–gel dip coated [11,16]. X-ray diffraction results confirmed that the CdO is the only phase inside these compounds. The lattice constant a was obtained from interplaner spacing of d_{hkl} value of the (1 1 1) and (2 0 0) peaks using the following equation [17]:

$$d_{hkl} = \frac{a}{\sqrt{h^2 + k^2 + l^2}}, \quad (1)$$

The mean value of the calculated lattice constant a for the undoped and Al-doped CdO is approximately equals 4.833 Å. The obtained data is in good agreement with JCDPS card No.78-0592 [18] which equal 4.694 Å.

X-ray diffraction measurements were used to determine the nature of the powder growth and the structural characteristics of undoped and Al-doped CdO. The crystallite size of the investigated materials can be calculated from the X-ray spectrum by means of full width at half maximum (FWHM) method known as Scherrer's equation [19]:

$$D = \frac{0.9\lambda}{\beta \cos\theta} \quad (2)$$

where β is the full-width at half maximum of the XRD peak appearing at the diffraction angle θ. The crystallite size of undoped and Al-doped CdO samples is given in Table 1. It is clear from Table 1

Table 1
The values of crystallite size D, strain ε and the dislocation density δ of pure and 5, 10, 15, 20% Al-doped CdO powder nanostructures.

	Crystallite size, D (nm)	Strain, ε ($\times 10^{-3}$) for (1 1 1) plane		The dislocation density, δ ($\times 10^{-5}$ Å^{-2})
		(1 1 1) plane	(2 0 0) plane	
Pure CdO	17.2	117.457	115.488	3.380
5% Al-doped CdO	15.9	124.165	124.934	3.956
10% Al-doped CdO	16.1	122.675	124.225	3.858
15% Al-doped CdO	16.3	121.477	121.155	3.764
20% Al-doped CdO	16.8	117.883	118.321	3.543

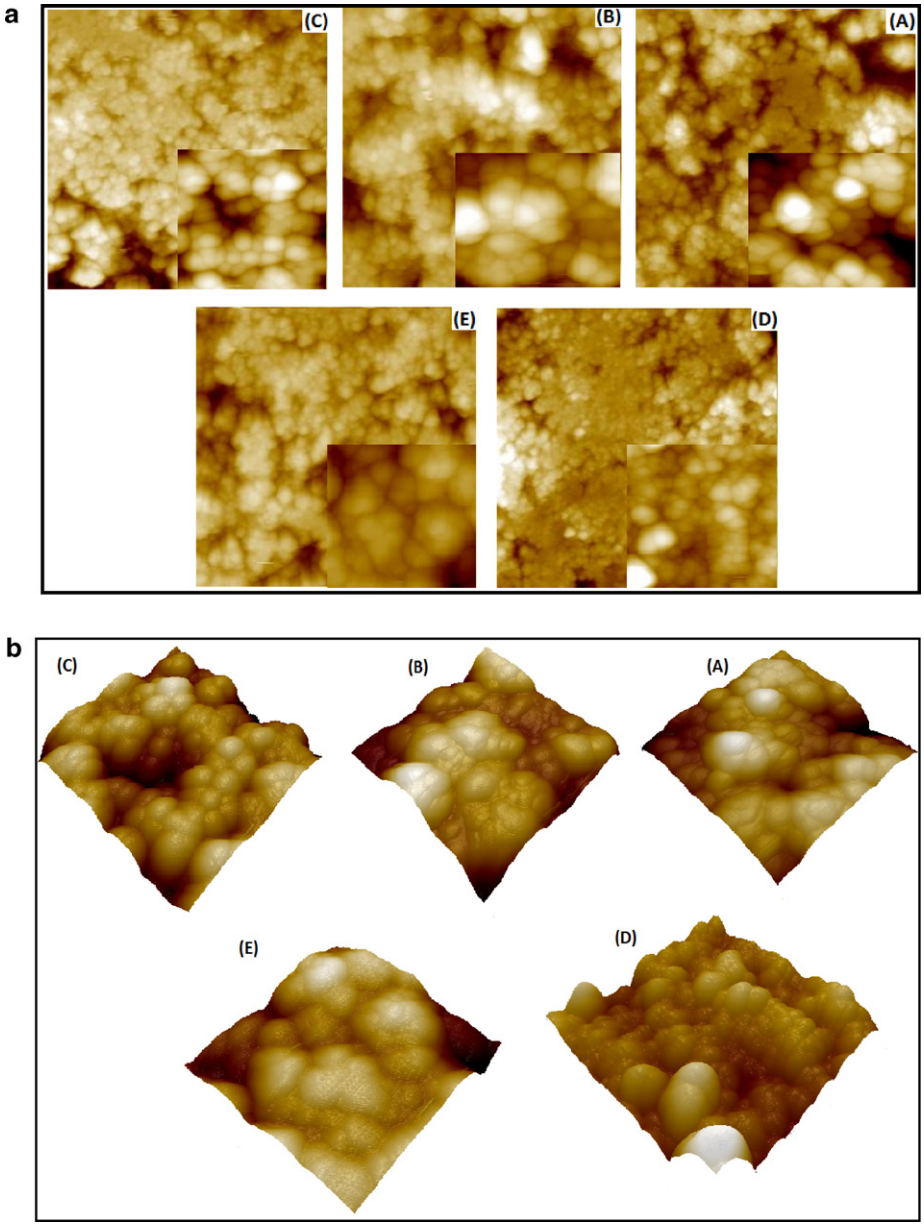

Fig. 3. (a) AFM images of (40 μm × 40 μm), inset: (5 μm × 5 μm) for (A) pure CdO, (B) 5%, (C) 10%, (D) 15% and (E) 20% Al-doped CdO powder nanostructures. (b) Three (3D) dimensional AFM images (5 μm × 5μm) for (A) pure CdO, (B) 5%, (C) 10%, (D) 15% and (E) 20% Al-doped CdO powder nanostructures.

that the crystallite size is changed unsystematically for a regular increase of aluminum concentration. Accordingly, it is possible to calculate both of the dislocation density δ, the strain ε and the texture coefficient T_c to have more information about the structure characteristics of undoped and Al-doped CdO nanostructured powders from the following equations [20–23]:

$$\delta = \frac{n}{D^2} \tag{3}$$

$$\varepsilon = \frac{\beta \cos\theta}{4} \tag{4}$$

$$T_c = \frac{I(hkl)/I_o(hkl)}{(1/N)\sum I(hkl)/I_o(hkl)} \tag{5}$$

where n is taken as unity at a minimum dislocation density, $I_o(hkl)$ is the intensity value of (hkl) plane from JCDPS card No. 78-0592, $I(hkl)$ is the measured intensity for each (hkl) plane and N is the number of diffraction peaks. The values of dislocation density δ and the strain ε of (1 1 1) and (2 0 0) planes for undoped and Al-doped CdO samples are given in Table 1. Fig. 2 shows the variation of the texture coefficient for different undoped and Al-doped CdO for (1 1 1), (2 0 0), (2 2 0), (3 1 1) and (2 2 2) planes. Among these planes, T_c(1 1 1) and T_c(2 0 0) exhibit the same trend as increased with increasing the Al-dopants of (10%) and then decreased again, while the other planes T_c(2 2 0), T_c(3 1 1) and T_c(2 2 2) show opposite trend, in which it is decreased until reached a minimum at Al-dopant of (10%) and then increased again. This indicates the occurrence of crystal reorientation effect due to the change of the Al-dopants concentration [24].

The structural properties of the Al doped CdO samples were investigated by AFM. The AFM images of (40 μm × 40 μm), inset: (5 μm × 5μm) and three (3D) dimensional for pure and Al-doped CdO samples are shown in Fig. 3a and b, respectively. As seen in Fig. 3a, the samples are consisted of nanoparticles in clusters (Nano-Particle Clusters). Type of nanostructure particles is like spherical as shown in Fig. 2b. The diameter of clusters of undoped and 5, 10,

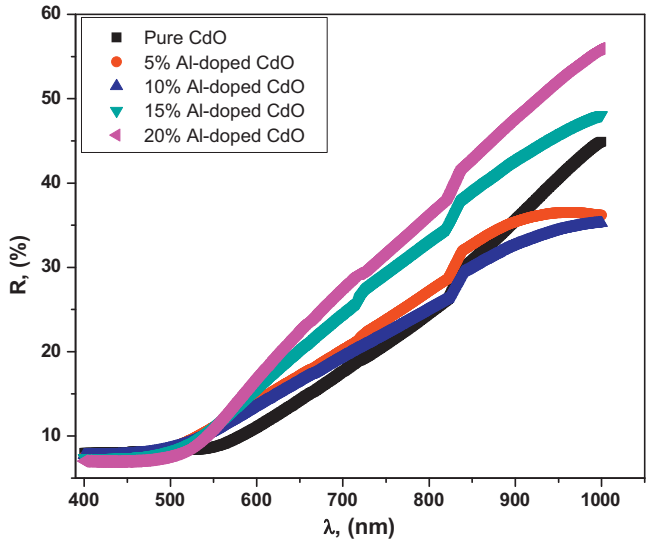

Fig. 4. The diffused reflectance of pure CdO, 5%, 10%, 15%, and 20% Al-doped CdO powder nanostructures.

15, 20% Al-doped CdO were 420, 335, 365, 350 and 330 nm, respectively. The diameter of the clusters is decreased with Al dopant except for 10% dopant.

3.2. Determination of optical band gap of pure and Al-doped CdO nanostructures

To determine the optical band gap of pure and Al-doped CdO nanostructures, the diffuse reflectance spectra for the powder samples were measured as shown in Fig. 4. As seen in Fig. 4, the reflectance of the samples increases with increasing the wavelengths. In order to determine the precise value of optical band gap of pure and Al-doped CdO nanostructures, the reflectance values were converted to absorbance by application of the Kubelka–Munk function [25–27]. The Kubelka–Munk theory is generally used for analyzing the diffuse reflectance spectra obtained from a weakly absorbing samples. It provides a correlation between reflectance and concentration. The concentration of an absorbing species can be determined using the Kubelka–Munk formula [25–27]:

$$F(R) = \frac{(1-R)^2}{2R} \tag{6}$$

where R is the diffused reflectance. $F(R)$ is Kubelka–Munk function which corresponds to the absorbance. $F(R)$ values were converted to the linear absorption coefficient by the following relation [27–29].

$$\alpha = \frac{F(R)}{t} = \frac{\text{Absorbance}}{t} \tag{7}$$

where t is the thickness of pure and Al-doped CdO. The optical transitions in semiconductor materials are taken place by direct and indirect transitions. The fundamental absorption, which corresponds to electron excitation from the valence band to conduction band, can be used to determine the value of the optical band gap E_g and it is related to the optical transition. The relation between the absorption coefficient α and the incident photon energy $h\upsilon$ can be written as [30,31]:

$$(\alpha h\upsilon) = A(h\upsilon - E_g)^n \tag{8}$$

where A is a constant depending on the transition probability and n is an index that characterizes the optical absorption process. The parameter n has the value 1/2 for the direct allowed transition and has the value 2 for the indirect allowed transition. Eq. (8) can be rewritten as [27]

$$\left(\frac{F(R)h\upsilon}{t}\right) = A(h\upsilon - E_g)^n \tag{9}$$

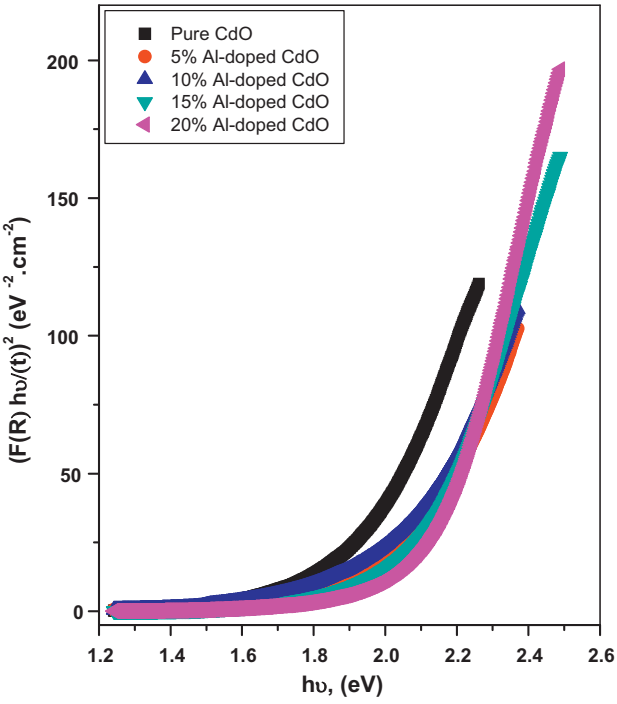

Fig. 5. The plot of $(F(R)h\upsilon)^2$ versus the photon energy for pure CdO, 5%, 10%, 15%, and 20% Al-doped CdO powder nanostructures.

The optical band gap values for pure and Al-doped CdO obtained by extrapolating the linear portion of the plots of $(F(R)h\upsilon/t)^2$ versus the photon energy to $h\upsilon = 0$ as shown in Fig. 5. These plots are shown in Fig. 5. The values of the obtained band gap E_g for pure and Al-doped CdO are given in Table 2. It is seen that the optical band gap of the samples slightly increases with the increase of Al content inside the pure samples. Generally, one can expect an increase in band gap of CdO doped with Al due to an increase in carrier concentrations which lead to the Burstein–Moss effect [32]. The optical band gap of the studied pure and Al-doped CdO samples is lower than the previously published work about the thin film samples of these compounds. Up to our knowledge, no data reported about the bandgap of the pure and Al-doped CdO nanopowders based on the diffused reflectance calculations.

3.3. Electrical conductivity of pure and Al-doped CdO nanostructures

Electrical conductivity reveals reliable information about the transport phenomenon of Al doped CdO samples. The electrical conductivities of pure and Al-doped CdO were measured in the temperature range (290–420 K) and their temperature dependence

Table 2
The values of the band gap and dc activation energy for pure and Al-doped CdO powder nanostructures.

Sample	E_g (eV)	σ_{RT} (S/cm) at 303 K	$E_{\sigma 1}$ (meV)	$E_{\sigma 2}$ (meV)
Pure CdO	1.89	227.854×10^{-3}	0.24	–
5% Al-doped CdO	2.07	69.029×10^{-3}	0.44	–
10% Al-doped CdO	2.03	43.836×10^{-3}	0.30	–
15% Al-doped CdO	2.07	46.254×10^{-3}	1.53	–
20% Al-doped CdO	2.12	147.365×10^{-3}	0.29	0.72

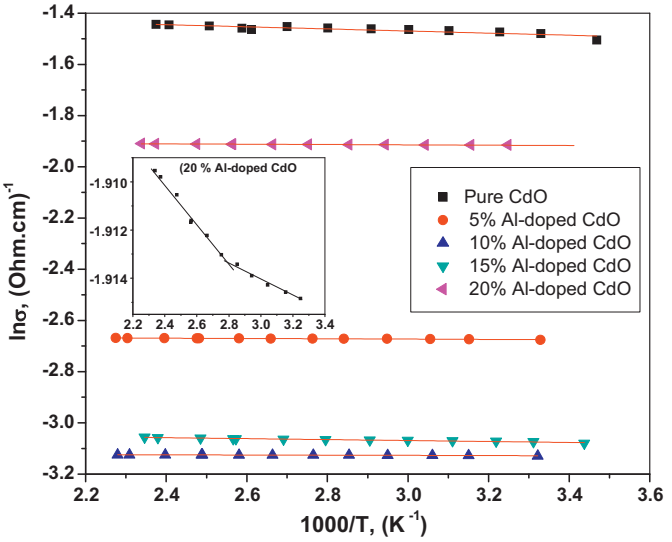

Fig. 6. Plots of $\ln\sigma$ vs $1000/T$ of pure CdO, 5%, 10%, 15%, and 20% Al-doped CdO powder nanostructures.

can be analyzed to the well known Arrhenius relation [33]:

$$\sigma_{dc} = \sigma_{o1} \exp\left(-\frac{\Delta E_{\sigma 1}}{k_B T}\right) + \sigma_{o2} \exp\left(-\frac{\Delta E_{\sigma 2}}{k_B T}\right) \quad (10)$$

where σ_{o1} is the pre-exponential factor, $\Delta E_{\sigma 1}$ is the activation energy in the low temperature range, σ_{o2} is the pre-exponential factor, $\Delta E_{\sigma 2}$ is the activation energy in the high temperature range and k_B is the Boltzmann constant. The plots of $\ln\sigma$ versus $1000/T$ for these powder nanostructures are shown in Fig. 6. These plots exhibit only one straight line for all the prepared samples associated with one conduction mechanism except for the 20% Al-doped CdO. The 20% Al-doped CdO exhibits two linear straight lines associated with two conduction mechanisms. The conductivity of these samples increases with increasing temperature showing the semiconducting behaviour of these powder nanostructures. The electrical conductivity results indicate that the electrical conduction mechanism is thermally activated processes and dc conductivity increases exponentially over the studied range of temperatures. The values of dc activation energies for the investigated compounds are listed in Table 2. As seen in Table 2, the electrical conductivity changes with Al dopant. The electrical conductivity of the samples is decreased with Al dopant. But, for the higher Al dopant, the electrical conductivity increases with respect to other dopants. This suggests that the electrical conductivity is controlled by the nanostructure.

4. Conclusions

Undoped and Al-doped CdO powder nanostructures were prepared by sol–gel calcinations method. XRD results indicate that pure and Al-doped CdO samples have the polycrystalline with nanostructure form. The values of particle size, strain, dislocation density and the texture coefficient are calculated based on the XRD data. The crystallite sizes for pure and Al-doped CdO are approximately in the same order even there is some changes with the change of Al-dopants. Accordingly, it is possible to control the nanostructure shape and size via sol–gel method and produced a high quality samples. The optical band gaps of undoped and 5, 10, 15, 20% of Al-doped CdO samples were found to be 1.89, 2.07, 2.03, 2.07 and 2.12 eV, respectively. The electrical conductivity mechanism of the samples is controlled by thermally activated processes. The obtained results indicate that Al-doped CdO samples are nanostructure powder materials.

Acknowledgements

This work was supported by the Management Unit of Scientific Research Projects of Firat University (FÜBAP) (Project Number: 1838). Authors wish to thank FÜBAP. This work was partially supported by the National Boron Research Institute (BOREN) (Grant No: BOREN-2009.Ç0226)

References

[1] S. Aksoy, Y. Caglar, S. Ilican, M. Caglar, Int. J. Hydrogen Energy 3 (4) (2009) 5191.
[2] K.R. Murali, A. Kalaivanan, S. Perumal, N. Neelakand Pillai, J. Alloys Compd. 503 (2010) 350.
[3] R. Ferro, J.A. Rodriguez, Sol. Energy Mater. Sol. Cells 64 (2000) 363.
[4] A.A. Dakhel, J. Alloys Compd. 504 (2010) 7.
[5] M.A. Flores, R. Castanedo, G. Torres, O. Zelaya, Solar Energy Mater. Solar Cells 93 (2009) 28.
[6] A. Wang, J.R. Babcock, N.L. Edleman, A.W. Metz, M.A. Lane, R. Asahi, V.P. Dravid, C.R. Kannewurf, PNAS 98 (2001) 7113.
[7] B. Li, L. Zeng, F. Zhang, Phys. Stat. Sol. A 201 (2004) 960.
[8] H.M. Ali, H.A. Mohamed, M.M. Wakkad, M.F. Hasaneen, Thin Solid Films 515 (2007) 3024.
[9] J. Santos Cruz, G. Torres Delgado, R. Castanedo Perez, C.I. Zuniga Romero, O. Zelaya Angel, Thin Solid Films 515 (2007) 5381.
[10] P.K. Ghosh, R. Maity, K.K. Chattopadhyay, Sol. Energy Mater. Sol. Cells 81 (2004) 279.
[11] R.K. Gupta, K. Ghosh, R. Patel, S.R. Mishra, P.K. Kahol, Curr. Appl. Phys. 9 (2009) 673.
[12] T.K. Subramanyam, S. Uthanna, B.S. Naidu, Mater. Lett. 35 (1998) 214.
[13] N. Ueda, H. Maeda, H. Hosono, H. Kawazoe, J. Appl. Phys. 84 (1998) 6174.
[14] B.J. Lokhande, P.S. Patil, M.D. Uplane, Mater. Chem. Phys. 84 (2004) 238.
[15] L.R. Gutierrez, J.J.C. Romero, J.M.P. Tapia, E.B. Calva, J.C.M. Flores, M.O. Lopez, Mater. Lett. 60 (2006) 3866.
[16] K.R. Murali, A. Kalaivanan, S. Perumalc, N. Neelakanda Pillai, J. Alloys Compd. 503 (2010) 350.
[17] G. Kittel, Introduction to Solid State Physics, fifth edition, John Wiley and Sons, New York, 1976.
[18] International Centre for Diffraction Data. JCDPS, PCPDFWIN, v. 2.3, 2002.
[19] B.D. Cullity, Elements of X-ray Diffraction, Addison-Wesley, Massachusetts, 1956.
[20] W.D. Callister, Materials Science and Engineering—An Introduction, John Wiley and Sons, New York, 1997.
[21] D.P. Padiyan, A. Marikini, K.R. Murli, Mater. Chem. Phys. 78 (2002) 51.
[22] K.R. Murali, A. Kalaivanan, S. Perumal, N. Neelakanda Pillai, J. Alloys Compd. 503 (2010) 350.
[23] C. Barret, T.B. Massalski, Structure of Metals, Pergamon, Oxford, 1980.
[24] R.J. Deokate, S.V. Salunkhe, G.L. Agawane, B.S. Pawar, S.M. Pawar, K.Y. Rajpure, A.V. Moholkar, J.H. Kim, J. Alloys Compd. 496 (2010) 357.
[25] A. Escobedo Morales, E. Sanchez Mora, U. Pal, Rev. Mexic. De Fisica S 53 (2007).
[26] V. Senthilkumar, P. Vickraman, R. Ravikumar, J. Sol–Gel Sci. Technol. 53 (2010) 316–321.
[27] F. Yakuphanoglu, J. Alloys Compd. 507 (2010) 184.
[28] A.E. Morales, E.S. Mora, U. Pal, Rev. Mex. Fis. 53 (5) (2007) 18–22.
[29] E. Yassitepe, Z. Khalifa, G.H. Jaffari, C.-S. Chou, S. Zulfiqar, M.I. Sarwar, S.I. Shah, Powder Technol. 201 (2010) 27.
[30] J.I. Pankove, Optical Processes in Semiconductors, Prentice-Hall, Englewood Cliffs, NJ, 1971.
[31] O.A. Azim, M.M. Abdel-Aziz, I.S. Yahia, Appl. Surf. Sci. 255 (2009) 4829.
[32] B. Saha, S. Das, K.K. Chattopadhyay, Solar Energy Mater. Solar Cells 91 (2007) 1692.
[33] Sh.A. Mansour, I.S. Yahia, F. Yakuphanoglu, Dyes Pigments 87 (2010) 144.